Computers & Structures Vol. 26, No. 6, pp. 1011–1025, 1987
Printed in Great Britain.

0045-7949/87 $3.00 + 0.00

CONCRETE MODEL WITH NORMALITY AND SEQUENTIAL IDENTIFICATION

F. B. LIN,† Z. P. BAŽANT,† J. C. CHERN‡§ and A. H. MARCHERTAS‡
†Center for Concrete and Geomaterials, Northwestern University, Tech, 2410, Evanston, IL 60201, U.S.A.
‡Division of Reactor Analysis and Safety, Argonne National Laboratory, 9700 South Cass Avenue, Argonne, IL 60439, U.S.A.

(*Received* 9 *December* 1986)

Abstract—To facilitate numerical finite element analysis, it is desirable to endow the constitutive model with normality, associatedness, continuity, convexity and absence of corners. Although these mathematical conditions represent only crude approximations of the actual behavior of concrete, it is of interest to find the best possible constitutive model which meets these conditons. This is one objective of the present paper. The second objective is to develop a model which permits a simple identification of material parameters from test data. The material parameters need not be obtained by simultaneous nonlinear optimization of the fits of all data. Rather, they are obtained in sequence through a precisely defined procedure which involves solving two systems of linear equations. The model describes not only hardening but also post-peak softening under various triaxial stress states. The model agrees well with the available basic test data from monotonic loading tests.

INTRODUCTION

The last dozen years have seen the development of a number of sophisticated constitutive models for nonlinear hardening and softening response of concrete[1–15]. The present paper develops yet another model, since the existing models still have some serious shortcomings. The material constants are not easily identified from the given test data, and infringements against the basic rules of classical plasticity in some of these models may cause certain numerical difficulties in finite element programs. The objective of the present model is to eliminate these two shortcomings.

The endochronic model [1, 2, 4, 5], whose first version, published in 1974, was perhaps the first realistic nonlinear triaxial model for concrete, requires that 15–20 independent material constants be determined simultaneously by non-linear optimization of data fits with a computer program for incremental loading. This task is surmountable but tedious and requires a specialist with a good deal of insight, experience and patience. No doubt this is the main reason why applications of this powerful theory have remained limited even though its use in small as well as large finite element programs has been proven workable [5, 16]. Moreover, certain discontinuities in the formulation have been perceived as a potential source of trouble with convergence, even though such troubles have not arisen in numerical applications [17]. Similar comments can be made about the plastic-fracturing theory [3] developed in 1977. A further shortcoming of these early models, which was not obvious from the experimental evidence at the time of their development, was that the post-peak strain-softening did not lead at very large strain to a complete reduction of the stress to zero (this will be assured by the present model).

Models that consist of a total stress–strain relation [6, 18], which should properly be enhanced by an additional path-dependent correction, might be most realistic for monotonic loading, but are discontinuous upon transitions to unloading. This makes their use in general-purpose finite element programs suspect. On the other hand, the existing models following the classical framework of plasticity, which ensures trouble-free numerical application, are quite limited in their data fitting capability and generally do not describe the post-peak softening.

The present paper, which represents a refinement and extension of a previous version by Chern *et al.* [19], seeks the best possible model whose material parameters can be easily identified from test data, and which at the same time adheres to the basic conditions of classical plasticity desired by numerical analysts: (1) normality rule (for the determination of the inelastic strain increments from a loading surface), (2) associatedness, (3) convexity of the loading surface, (4) continuity and (5) smooth loading surface, i.e. absence of corners.

Gratifying though the attainment of these objectives might be, we must nevertheless keep in mind that the reality is more demanding. A complete description of concrete would certainly require multiple loading surfaces and deviations from normality, etc. due to internal friction and microcracking. Moreover, a constitutive model *per se*, no matter how sophisticated, cannot provide a complete description

§Visiting Scholar, Northwestern University; present address: Department of Civil Engineering, National Taiwan University, Roosevelt Rd., Sec. 4, Taipei, Taiwan.

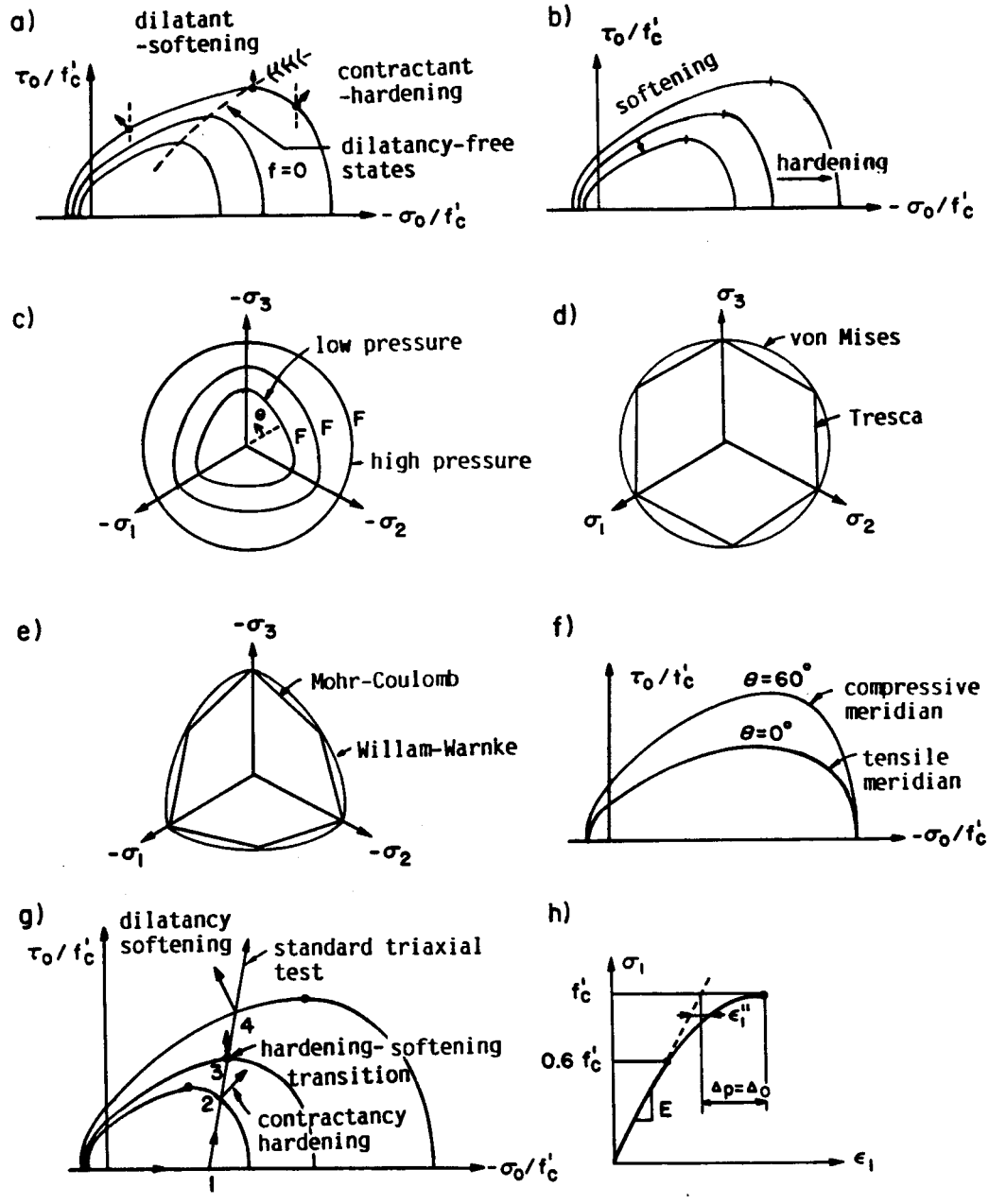

Fig. 1. Loading surfaces of various properties.

of concrete. As transpires from the latest research on strain localization instabilities due to strain-softening [20, 21], the constitutive model must be combined in some way with a fracture mechanics approach which captures the nonlocal properties of the material and serves to restrict the localization of strain-softening to a finite volume. Due to the neglect of these aspects, which are beyond the scope of the present paper, we cannot expect a very close agreement with all test results.

LOADING SURFACE

As an acceptable approximation, concrete may be assumed to be isotropic. The dependence of the loading surface on the stress tensor σ then reduces to a dependence on the stress invariants. There are three independent stress invariants; we will use the mean stress σ_0 (identical to the octahedral normal stress), the octahedral shear stress τ_0, and the similarity angle θ; they are defined as

$$\sigma_0 = \tfrac{1}{3}I_1, \quad \tau_0 = \sqrt{\tfrac{2}{3}J_2}, \quad \cos 3\theta = \frac{3\sqrt{3}}{2} J_3 J_2^{-3/2} \quad (1)$$

in which $I_1 = \sigma_{kk}$ = first invariant of stress tensor σ whose Cartesian components are σ_{ij}, $J_2 = s_{ij}s_{ij}/2$ = second invariant of the stress deviator $s_{ij} = \sigma_{ij} - \delta_{ij}\sigma_o$, $J_3 = s_{ij}s_{jk}s_{ki}/3$ = third invaiant of s_{ij}. The lower case subscripts refer to Cartesian coordinates x_i

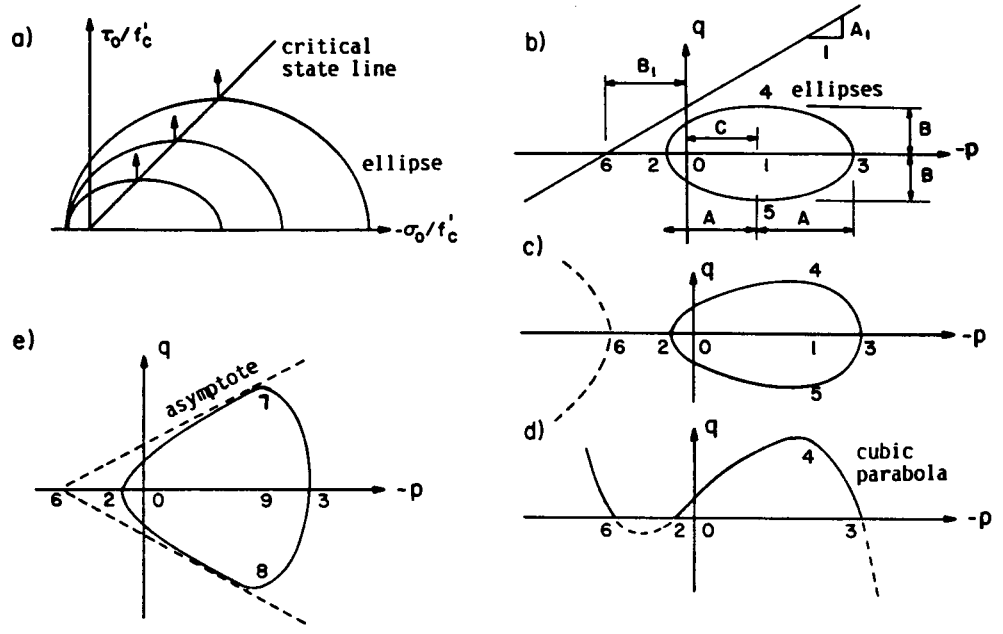

Fig. 2. Ellipse of critical state theory of soils and generation of the present slanted ellipse surface (shaded).

($i = 1, 2, 3$), Einstein's summation rule is assumed, and δ_{ij} = Kronecker's delta. Angle θ represents the polar angle in the deviatoric section, measured from the positive σ_1 direction, σ_1, σ_2 and σ_3 being the principal stresses. Always $0 \leq \theta \leq \pi/3$ [Fig. 1(c)].

The loading surface which we plan to formulate must expand at small deformations to describe initial hardening (as compared to perfect yield), and contract at large deformations to describe progressive damage or softening. In the volumetric cross-section (σ_0, τ_0) of the principal stress space (σ_1, σ_2, σ_3), called the Rendulić plane, the surface must be asymmetric, since the strength in compression is greater than in tension, and must initially have a positive slope as the hydrostatic compression $-\sigma_0$ is increased, similar to the Mohr–Coulomb or Drucker–Prager yield criteria. At high hydrostatic compression $-\sigma_0$, however, the loading surface must drop to the $-\sigma_0$ axis. In connection with the Drucker–Prager yield criterion, this drop has been described in other works by a separate surface called the cap, which usually forms a corner with the Drucker–Prager surface. However, we want to avoid using a corner because it complicates the formulation. We avoid it most easily, while still preserving the basic frictional-dilatant characteristics, if we formulate the Rendulić section as an eccentric ellipse [Fig. 2(a)]. Such an ellipse has been widely used in soil plasticity and has been called the critical state theory [22]. The critical state is a term used for the peak point of the ellipse, for which the normality rule indicates zero plastic dilatation and zero plastic compaction. This characteristic is quite critical for soil response, but not as critical for concrete or rock.

The ellipse, borrowed from the critical state theory of soils, provides an attractive simple loading surface, which was recently adapted for concrete by Zubelewicz and Bažant [15]. The shape of the ellipse, however, is not ideal. We need a surface whose rise towards the peak is closer to a straight line and which drops after the peak toward zero more rapidly than an ellipse. This feature (which was achieved in Zubelewicz and Bažant's work by rotation of the so-called active plane) will be achieved in the present model by slanting the ellipse to an egg-shaped surface as shown in Fig. 2c.

The slanting of the ellipse is easily achieved by multiplying the equation for the ellipse by an equation for an inclined straight line which intersects the tension axis outside the ellipse, at point 6 in Fig. 2(b). The ellipse, one axis of which lies on the hydrostatic axis, is given by the equation

$$\left(\frac{q}{B}\right)^2 = 1 - \left(\frac{p+C}{A}\right)^2 \tag{2}$$

in which p and q are the nondimensional mean normal and shear stresses

$$p = \sigma_0/f'_c, \quad q = \tau_0/f'_c \tag{3}$$

normalized with respect to the uniaxial compression strength f'_c. A, B, C are parameters of the ellipse; $p = -C$ gives the center of the ellipse, $p = -C \pm A$ gives the apices on the p-axis, and B is the semi-axis of the ellipse in the shear direction q [Fig. 2(b)].

To slant the ellipse into an egg shape, we multiply the right-hand side of eqn (2) with the equation of the straight line, $q = A_1(B_1 + p)$, in which [Fig. 2(b)] A_1 is the slope of the line and the point $p = -B_1$ is the intersection point with the tension axis $-p$. If the straight line intersected the p-axis between the apices of the ellipse, which would occur for $B_1 < A - C$, the

loading surface would have the shape of a figure of eight. To prevent it, we require $B_1 > A - C$. Thus, the equation of the slanted ellipse has the form

$$q = B\left\{\left[1 - \left(\frac{p+C}{A}\right)^2\right](B_1 + p)\right\}^{1/2} \tag{4}$$

or

$$q = (\alpha_0 + \alpha_1 p + \alpha_2 p^2 + \alpha_3 p^3)^n \tag{5}$$

in which $n = 1/2$, $\alpha_0 = B_1(A^2 - C^2)/\alpha_3$, $\alpha_1 = (C^2 - A^2 + 2B_1C)\alpha_3$, $\alpha_2 = -(2C + B_1)\alpha_3$, and $\alpha_3 = B^2/A^2$. For the sake of generality, one could allow a general exponent n such that $0 < n < 1$. Equation (5) is equivalent to eqn (4) only if $n = 1/2$, and this value has been used for all data fitting.

Note that the slanted ellipse, shown in Fig. 2(c), may be also obtained by taking the square root of the positive values of a cubic parabola such that $\alpha_3 > 0$. Axis p is intersected at three points, which requires that $4\alpha_2^2 - \alpha_1 > 0$ [Fig. 2(c)]. This reveals that eqns (4) or (5) give a two-branch curve. The second branch is open. It is shown as the dashed curve in Fig. 2(c) and is discarded for our purposes. The p-coordinate of the peak point of the slanted ellipse, point 4 in Fig. 2(c), is obtained by setting $\partial q/\partial p = 0$, which yields

$$[p]_{\max q} = p_0 = -\frac{1}{3\alpha_3}\left(\alpha_2 + \sqrt{\alpha_2^2 - \frac{\alpha_1}{4}}\right). \tag{6}$$

This value is real under the conditon $4\alpha_2^2 - \alpha_1 > 0$ stated before.

Equations (4) or (5) do not necessarily yield a convex curve. Convexity is obtained only if the p-intercept of the straight line is sufficiently remote from the ellipse apex in Fig. 2(b), or more precisely if the ratio $\overline{2\,6}/\overline{1\,2}$ is not too small, i.e. $(B_1 + C)/A$ is sufficiently large. Denote by $p_{(1)}$ and $p_{(2)}$ the smallest two roots of the cubic polynomial in eqn (5) which represent the abscissae of the right and left apices of the slanted ellipse [Fig. 2(c)]. By affinity transformations with regard to axis p and axis q and translation in the p direction, one can prove that eqn (5) is convex between $p_{(1)}$ and $p_{(2)}$ if and only if the curve $y = [x(1-x)(x+c)]^n$ with $c = (p_{(3)} - p_{(2)})/(p_{(2)} - p_{(1)})$ is convex for $0 \le x < 1$. Calculating the limiting values of c for various n and fitting them with a polynomial, one can show that the condition of convexity is:

for

$$\begin{aligned} &n \le 0.5: && c \ge 0 \\ &n = 0.51: && c \ge 0.003 \\ &n = 0.6: && c \ge 0.057 \\ &n = 0.7: && c \ge 0.145 \\ &n = 0.8: && c \ge 0.260. \end{aligned} \tag{7}$$

The slanted ellipse formulation is needed particularly to describe the inelastic response at large strain, which consists predominantly of microcracking (at high shear stress) or pore collapse (at high hydrostatic compression) and results in significant inelastic volume changes which soften or harden the material. The loading surface may be written in the form

$$F(\sigma) = \sqrt{3}\tau_0 - r(\theta, p, \tau) \tag{8}$$

in which τ will be used as a hardening–softening parameter. This surface will be assumed to coincide with inelastic potential whose normal yields the direction of the inelastic strain increment. In other words, we assume perfect normality.

(a) *Deviatoric section.* As is now well documented, the deviatoric section of a loading surface or potential for concrete as well as geomaterials should have only three rather than six axes of symmetry. For example, the hexagon for the Tresca criterion [Fig. 1(d)] should be generalized to the irregular hexagon for the Mohr–Coulomb criterion [Fig. 1(e)]. The presence of corners in the hexagon, however, is inconvenient for numerical analysis and a smooth surface is preferable. Among simple surfaces, the circular von Mises-type deviatoric section, assumed in the Drucker–Prager criterion, is unrealistic for concrete. The deviatoric section should have the form of a rounded triangle shown in Fig. 1(c), which is closer to a triangle (sharper vertices) at small hydrostatic pressures and closer to a circle for high hydrostatic pressures. These properties are documented by many data, the first of which were probably those of Launay and Gachon [23].

The earliest and shortest expression for the rounded triangular deviatoric section was given simultaneously by Gudehus [24] and Argyris *et al.* [25]. However, as recently pointed out by Lin and Bažant [26], this expression does not give a convex curve when the ratio of the radial distances for the tensile and compression meridians in the deviatoric planes becomes too small (less than about 0.777), as required for concrete at small hydrostatic pressures. Therefore, we use a slightly more complicated two-parameter formula which was proposed by Willam and Warnke [27] as part of their five-parameter yield criterion for concrete failure. This formula guarantees convexity because for each sector $0 \le \theta \le 60°$ in the deviatoric section it represents a segment of an ellipse, and these segments are matched so that the slope is continuous. In terms of two independent parameters r_c and r_t, representing the radial distances to the compression meridian ($\theta = 60°$) and to the tensile meridian ($\theta = 0$), Willam–Warnke's formula may be written as:

$$r(\theta, p, \tau) = r_c \frac{R + (2r_t - r_c)(2R\cos\theta + 5r_t^2 - 4r_t r_c)^{1/2}}{2R\cos\theta + (2r_t - r_c)^2},$$
$$R = 2(r_c^2 - r_t^2)\cos\theta. \tag{9}$$

(b) *Shear-volumetric (Rendulić) sections.* Following the egg-shaped slanted ellipse defined by eqn (5), the radial distances vary along the compression and tensile meridians as follows ($n = 1/2$).

Tensile meridian ($\theta = 0$):

$$r_t = \sqrt{3}\,\tau\left[\alpha_0 + \alpha_1\frac{\sigma_0}{\tau} + \alpha_2\left(\frac{\sigma_0}{\tau}\right)^2 + \alpha_3\left(\frac{\sigma_0}{\tau}\right)^3\right]^n \quad (10)$$

Compression meridian ($\theta = 60°$):

$$r_c = \sqrt{3}\tau\left[\beta_0 + \beta_1\frac{\sigma_0}{\tau} + \beta_2\left(\frac{\sigma_0}{\tau}\right)^2 + \beta_3\left(\frac{\sigma_0}{\tau}\right)^3\right]^n, \quad (11)$$

where τ determines the size of the loading surface (initially $\tau = 0.6f_c'$).

These equations involve eight parameters $\alpha_0, \ldots, \alpha_3, \beta_0, \ldots, \beta_3$. However, only six of them are independent since the two apices of each slanted ellipse meridian on the p-axis must be common to both meridians [Fig. 1(f)]. This means that the smallest two roots of the cubic polynomial in eqn (10) must be the same as for eqn (11), while the third and largest root may be different.

HARDENING AND SOFTENING RULES

We must now define the rules for hardening and softening which describe how the loading surface changes due to inelastic strain that has taken place. To make a simple, sequential identification of material parameters possible, we will assume that the loading surface defined by eqns (8)–(11) can only expand or shrink radially. This is called the isotropic hardening and is described by a variation of parameter τ. When plotted as σ_0/τ vs r_c/τ or σ_0/τ vs r_t/τ, the loading surface is a single, fixed curve.

The isotropic hardening, to be sure, is a simplification. In reality, the loading surface may also translate and change its shape. Shape changes could be described by a variation of parameters $\alpha_0, \alpha_1, \ldots, \beta_2, \beta_3$. Such a generalization, however, would not only be too complicated but also offer only a limited improvement, since in reality one must expect many simultaneously active loading surfaces, all of them varying their sizes and shapes. Moreover, the existing data seem insufficient to determine any rules for variation of $\alpha_0, \ldots, \beta_3$.

(a) *Deviatoric hardening.* In uniaxial compression, the inelastic strain becomes appreciable at about $0.6f_c'$. Therefore, we set the initial value of τ as $0.6f_c'$, and for the peak stress state we have $\tau = f_c'$. Since the loading surface will be calibrated from the peak stress values for various multiaxial types of test, the value $\tau = f_c'$ also indicates the peak stress in other types of tests, provided they exhibit a peak point. The variation of τ from $0.6f_c'$ to f_c' characterizes the hardening stage of inelastic response, which is known to be predominantly deviatoric; see Gerstle *et al.* [18] and others [8, 28, 29]. Therefore we assume the initial hardening to be deviatoric, characterized in terms of the effective strain $\bar{\epsilon}''$, which may be defined in an invariant manner by the work equality $\tau\,d\bar{\epsilon}'' = \sigma_{ij}\,d\epsilon_{ij}''$, from which

$$d\bar{\epsilon}'' = \frac{\sigma_{ij}\,d\epsilon_{ij}''}{\tau}, \quad (12)$$

where ϵ_{ij}'' is the inelastic strain. Equation (12) is guaranteed to be non-negative because, for hardening, Drucker's postulate is satisfied by our model. Since $\bar{\epsilon}''$ approximately coincides with the axial inelastic strain $\epsilon_1'' = \epsilon_1 - \sigma_1/E$, we have $d\bar{\epsilon}''/d\tau = \phi'(\tau) = 1/H$, where function $\phi(\tau)$ may be considered identical to the plastic strain part of the uniaxial compression curve ϵ_1/σ_1, i.e. $\phi(\sigma_1) = \epsilon_1(\sigma_1) - \sigma_1/E$; $\phi'(\sigma_1) = d\phi/d\sigma_1$, and H is called the plastic hardening modulus; $H = d\tau/d\bar{\epsilon}'' = d\sigma_1/d\epsilon_1''$. The deviatoric hardening rule for the initial inelastic behavior may be expressed as $d\tau = H(\tau, \sigma_0, \bar{\epsilon}'')d\bar{\epsilon}''$ (for $d\bar{\epsilon}'' > 0$, $0.6f_c' \le \tau < f_c'$).

To describe the variation of H, one may assume the rising part of the uni-axial compression curve for $0.6f_c' \le \sigma_1 \le f_c'$ to be a quarter-ellipse, i.e. $(\tau - 0.6f_c')^2/(0.4f_c')^2 + (\Delta_p - \bar{\epsilon}'')^2/\Delta_p^2 = 1$, in which τ is substituted for the octahedral shear stress τ_0 and Δ_p = horizontal offset of the peak stress point from the intial elastic tangent [Fig. 1(h)]. Calculating $H = d\tau/d\bar{\epsilon}''$ from this equation, the deviatoric hardening rule takes the particular form:

$$d\tau = H\,d\bar{\epsilon}'' = \left(\frac{0.4f_c'}{\Delta_p}\right)^2\frac{\Delta_p - \bar{\epsilon}''}{\tau - 0.6f_c'}\,d\bar{\epsilon}'', \quad (0.6f_c' < \tau \le f_c'). \quad (13)$$

Although the elastic limit is considered as $0.6f_c'$ in all the present calculations, note that by changing it one could control the curvature of the stress–strain diagram at the peak stress point. Another possibility (used in most calculations) is to define the curve $\tau(\bar{\epsilon}'')$ by a set of points on the basis of the uniaxial curve $\sigma_1(\epsilon_1)$, and interpolate between these points.

By defining the effective plastic strain, eqn (12), we can extrapolate from the uniaxial stress–strain curve to the stress–strain curve under any multiaxial loading. The peak points of these curves agree with test results quite well because they are based on one loading surface, eqns (8)–(11), which is made to fit the maximum stress states at various types of multiaxial loading. If, however, Δ_p is assumed to be constant for all multiaxial loadings, the strains at the maximum stress state are then found to differ from the test data considerably for some multiaxial loadings. For example, for the proportional triaxial tests of van Mier, the strain at peak was much less than he observed, while the peak stress value was predicted correctly. This experience indicates that the peak point offset Δ_p must be considered as variable. In particular, Δ_p appears to be a function of the similarity angle θ, such that Δ_p is maximum for $\theta = 60°$ (uniaxial compression) and minimum for $\theta = 0$ (biaxial compression or uniaxial tension). This may be described by introducing in eqn (13) the following empirical function:

$$\Delta_p = \Delta_0[\alpha + (1-\alpha)\sin^m \tfrac{3}{2}\theta] \quad (14)$$

with $m = 2$, and Δ_0, α are positive constants ($\alpha < 1$), Δ_0 is the peak stress offset for the uniaxial compression curve [Fig. 1(i)] and Δ_p is the peak offset for the effective stress–strain curve $\tau(\bar{\epsilon}'')$.

(b) *Volumetric hardening*. After the peak stress, i.e. after τ has already reached the value of f_c', the loading surface must shrink in order to describe the post-peak strain-softening. This means that the value of τ must decrease. However, if there is high hydrostatic compression, no peak exists on the stress–strain curve; rather, there is continued hardening, i.e. the loading surface continues to expand and τ grows beyond the value of f_c'. In this case, as well as in the cases with a peak, the value $\tau = f_c'$ corresponds to the critical state at which $d\epsilon_0''$ vanishes, i.e. the inelastic expansion is zero (which in soil mechanics is called the critical state). In the second stage of inelastic behavior, the softening as well as hardening is dominated by inelastic volumetric strain $\epsilon_0'' = \epsilon_{kk}''/3$. This strain corresponds to tensile microcracking in the case of softening, and to pore collapse in the case of hardening.

When the volumetric inelastic strain ϵ_0'' is negative (compressive), i.e. when the current state point is to the right of the peak of slanted ellipse, the pores are closing due to their collapse. So, the material hardens, i.e. τ increases. Experience shows that the following simple expression may describe this adequately:

$$d\tau = -\lambda_1 \tau d\epsilon_0'' \quad (\text{hardening}, \epsilon_0'' \le 0) \quad (15)$$

in which λ_1 is an empirical parameter; the initial value is $\tau = f_c'$. In an integrated form, $\tau = \tau_1 \exp(-\lambda_1 \epsilon_0'')$. The hardening coefficient λ_1 may be identified on the basis of hydrostatic compression data. This hardening causes an expansion of the slanted elliptic surface, as shown in Fig. 1b.

The softening due to microcracking, which is accompanied by inelastic volume expansion, results in a decrease of τ, manifested by shrinking of the slanted ellipse as shown in Fig. 1(b). This may be approximately described, as data fitting confirmed, by the simple expression;

$$d\tau = -2\lambda\tau\epsilon_0'' \, d\epsilon_0'' \quad (\text{softening}, d\epsilon_0'' > 0). \quad (16)$$

For constant λ, this equation may be integrated as $\tau = \tau_1 \exp(-\lambda^2 \epsilon_0''^2)$. It appears that for large enough $|\sigma_0|$ the value of λ may be considered as constant, $\lambda = \lambda_t$ for tension ($\sigma_0 > 0$), and another constant $\lambda = \lambda_c$ ($\sigma_0 < 0$) for compression ($\sigma_0 < 0$). Typically, $\lambda_t \simeq 10\,\lambda_c$.

The transition between hardening and softening defined by eqns (15)–(16) is continuous because for $d\epsilon_0'' \to 0$ there is no hardening or softening. The transition between softening under tension ($\sigma_0 > 0$ and $\epsilon_0'' > 0$) and softening under compression ($\sigma_0 < 0$ and $\epsilon_0'' > 0$) would be discontinuous if λ were equal to λ_t for all tension states, and λ_c for all compression states. Therefore we choose a continuous transition from λ_c to λ_t such that

$$\lambda = \lambda_t + (\lambda_c - \lambda_t)\left(\tfrac{1}{2} + \tfrac{1}{2}\tanh\frac{10\sigma_0}{\tau}\right)^3. \quad (17)$$

Temperature and moisture effects could be introduced by means of additional rules for the variation of parameter τ.

NORMALITY RULE AND CONTINUITY

Lest problems with convergence would be encountered in computation, we prefer to adhere to the normality rule even though it is not necessarily applicable to materials that exhibit internal friction and microcracking. Thus, in analogy to classical plasticity, we assume:

$$d\epsilon_{ij}'' = \frac{\partial G}{\partial \sigma_{ij}} \langle d\lambda \rangle \quad (G \equiv F) \quad (18)$$

in which $G(\boldsymbol{\sigma})$ represents the inelastic potential surfaces, and $\langle d\lambda \rangle = d\lambda$ if $d\lambda > 0$ and $\langle d\lambda \rangle = 0$ if $d\lambda \le 0$. Equation (18) with $d\lambda = (\partial F/\delta\sigma_{km})\, d\sigma_{km}$ (where F = loading surface) was proposed as early as 1938 by Melan [30].

Since fulfilment of Drucker's stability postulate is not a necessary condition for materials with microcraking and friction, the potential G could in general be different from the loading surface F, which would represent a non-associated normality rule analogous to the classical non-associated plasticity. Again, however, it is preferable for computational reasons to assume an associated normality rule. Aside from that, no strong experimental evidence seems to require non-associatedness. Therefore, in all calculations with the present model we assume that $G \equiv F$.

The total strain increment may now be expressed as

$$d\epsilon_{ij} = d\epsilon_{ij}^e + d\epsilon_{ij}'' + d\epsilon_{ij}^{th} + d\epsilon_{ij}^{sh} + d\epsilon_{ij}^{cr} \quad (19)$$

in which $d\epsilon_{ij}^e$ represents the elastic strain increment, and $d\epsilon_{ij}^{th}$, $d\epsilon_{ij}^{sh}$ and $d\epsilon_{ij}^{cr}$ are the thermal, shrinkage and creep strains, the formulation of which is beyond the scope of the present paper. The stress can be expressed in terms of the elastic strain as $\sigma_{ij} = C_{ijkm}\epsilon_{km}^e$ in which C_{ijkm} are the elastic moduli. By differentiation, the incremental elastic relation is

$$d\sigma_{ij} = C_{ijkm}\, d\epsilon_{km}^e + dC_{ijkm}\epsilon_{km}^e \quad (20)$$

in which

$$dC_{ijkm} = \frac{\partial C_{ijkm}}{\partial T} dT + \frac{\partial C_{ijkm}}{\partial h} dh. \quad (21)$$

Here we take into account the fact that in concrete the elastic moduli generally depend on temperature T

Table 1. Basic conditions from which material constants are determined

Material characteristic	Stress state	p	q	θ	r
1. Uniaxial tensile strength	$\sigma_1 = f'_t, \sigma_2 = \sigma_3 = 0$	$\rho_{tc}/3$	$\rho_{tc}\sqrt{2}/3$	0	r_t
2. Uniaxial compression strength	$\sigma_3 = -f'_c, \sigma_1 = \sigma_2 = 0$	$-1/3$	$\sqrt{2}/3$	60°	r_c
3. Biaxial compression strength	$\sigma_2 = \sigma_3 = -f'_{cb}, \sigma_1 = 0$	$-2\rho_{cb}/3$	$\rho_{cb}\sqrt{2}/3$	0	r_t
4. Hydrostatic elastic limit	$\sigma_1 = \sigma_2 = \sigma_3 = -f'_{ce}$	ρ_{ce}	0	0 or 60°	$r_t = r_c = 0$
5. Dilatancy-free state at tensile meridian	$\partial q/\partial p = 0$	p_t	r_t	0	$r_t = r_{min}$
6. Dilatancy-free state at compression meridian	$\partial q/\partial p = 0$	p_c	r_c	60°	$r_c = r_{max}$

and pore relative humidity h. We neglect any effect of microcracking damage on the elastic moduli since microcracking is taken into account in our model in terms of the loading surface. If we considered damage, dC_{ijkm} would also depend on $d\epsilon_{ij}$, but this we neglect for the sake of simplicity.

To maintain a continuous inelastic deformation, the current stress point must remain on the loading surface, which requires that $F = 0$ holds true through subsequent loading stages. Thus we have for the inelastic deformation the continuity condition $dF = 0$, which may be rewritten as

$$\frac{\partial F}{\partial \sigma_{ij}} d\sigma_{ij} + \frac{\partial F}{\partial \tau} = 0,$$

with

$$d\tau = \frac{\partial \tau}{\partial \epsilon''_0} d\epsilon''_0 + \frac{\delta \tau}{\partial \bar{\epsilon}''} d\bar{\epsilon}'' + \frac{\partial \tau}{\partial T} dT + \frac{\partial \tau}{\partial h} dh. \quad (22)$$

The continuity condition, proposed already by Prager, is again not a strict requirement (see, e.g. [31]), but its violation might cause numerical problems. Note that the first two terms in eqn (22) for $d\tau$ cannot be both non-zero, according to our definition of the hardening–softening rules.

To express the proportionality coefficient $d\lambda$, we may now substitute eqns (19), (20) and (18) into eqn (22) and the resulting equation for $d\lambda$. In the calculations we note that $\partial \epsilon''_0 / \partial \epsilon''_{ij} = \delta_{ij}/3$. For volumetric hardening or softening we thus obtain:

$$d\lambda = \left\langle \frac{\frac{\partial F}{\partial \sigma_{ij}} (C_{ijkm} d\epsilon^e_{km} + dC_{ijkm} \epsilon^e_{km}) + \frac{\partial F}{\partial \tau} \left(\frac{\partial \tau}{\partial T} dT + \frac{\partial T}{\partial h} dh \right)}{\frac{\partial F}{\partial \sigma_{ij}} C_{ijkm} \frac{\partial G}{\partial \sigma_{km}} - \frac{\partial F}{\partial \tau} \frac{\partial \tau}{\partial \epsilon''_{ij}} \frac{\partial G}{\partial \sigma_{ij}}} \right\rangle. \quad (23)$$

Our formulation is now complete. The incremental constitutive equation is given by eqn (19) with the elastic strain satisfying eqns (20)–(21), the inelastic strain increments given by eqn (18) with the proportionality coefficients according to eqn (23), the loading surface evolution according to eqns (13), (15), (16), and the hardening–softening rules given by eqns (15), (16). The constitutive model involves a total of 14 independent constants to be identified from test data. They comprise parameters $\alpha_0, \ldots, \alpha_3, \beta_0, \ldots, \beta_3$, among which only six are independent, parameters λ_1, λ_c, λ_t, Δ_0 and α, standard compression strength f'_c, and Young's and shear moduli E and G from which the tensor C_{ijkm} is determined. This is nearly as many constants as needed in the previous nonlinear constitutive models which give good descriptions of concrete, such as the endochronic model, the plastic-fracturing model, Dafalias' bounding surface model and others [14].

After extensive efforts it now seems that trying to do with only few material constants is futile as long as one adheres to the macroscopic approach. A drastic reduction in the number of material constants might perhaps be possible by means of micromechanic models, such as the microplane model [32], however, at the price of a considerable increase of computational work.

The material constants in the present model are nevertheless easier to identify from test data than those of previous more sophisticated models giving good descriptions of concrete. While in such previous models the material parameters had to be determined in essence simultaneously, by concurrent optimization of the fits of many different types of data, our new model permits that the material constants be identified from the material experimental characteristics sequentially, with little difficulty.

IDENTIFICATION OF MATERIAL CONSTANTS

In Table 1 we propose a set of six basic material characteristics which are graphically illustrated in Fig. 3. They can be directly obtained by measurements and suffice for determining material constants $\alpha_0, \ldots, \alpha_3, \beta_0, \ldots, \beta_3$. It is useful to define the nondimensional strength ratios

$$\rho_{tc} = f'_t/f'_c, \quad \rho_{cb} = f'_{cb}/f'_c, \quad \rho_{ce} = f'_{ce}/f'_c \quad (24)$$

in which f'_t = uniaxial tensile strength, f'_{cb} = biaxial compression strength and f'_{ce} = hydrostatic pressure at the elastic limit in hydrostatic compression. This state corresponds to the beginning of inelastic volume compaction due to pore collapse.

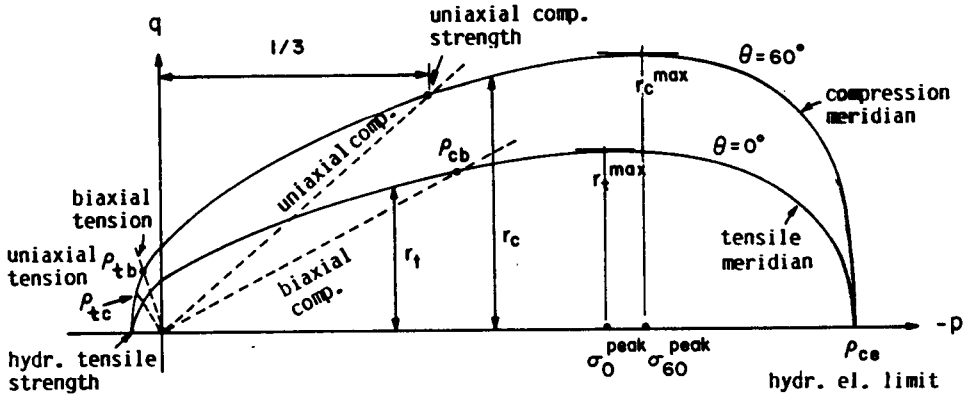

Fig. 3. Basic strength data and characteristic stress states used for identification of the compression and tensile meridians of the loading surface.

The dilatancy-free states in rows 5 and 6 of Table 1 are analogous to the critical states in soil mechanics. The dilatancy-free state at the tensile meridian (row 5) may be obtained by running a biaxial compression test and measuring the volume change to determine the last point at which the rate of inelastic volume increase is zero. The dilatancy-free state at the compression meridian (row 6) may be determined similarly from a uniaxial compression test in which the inelastic volume change is measured. The useful property of the characteristics in Table 1 is that the states in rows 1, 3, 4 and 5 depend only on the tensile meridian, eqn (10). Substituting the stress states from these rows into eqn (10) and its derivative, we obtain for constants $\alpha_0, \ldots, \alpha_3$ of the tensile meridian a system of four linear algebraic equations:

$$\begin{aligned} \alpha_0 + \tfrac{1}{3}\rho_{tc}\alpha_1 + \tfrac{1}{9}\rho_{tc}^2\alpha_2 + \tfrac{1}{27}\rho_{tc}^3\alpha_3 &= \tfrac{2}{9}\rho_{tc}^2 \\ \alpha_0 - \tfrac{2}{3}\rho_{cb}\alpha_1 + \tfrac{4}{9}\rho_{cb}^2\alpha_2 - \tfrac{8}{27}\rho_{cb}^3\alpha_3 &= \tfrac{2}{9}\rho_{cb}^3 \\ \alpha_0 + \rho_{ce}\alpha_1 + \rho_{ce}^2\alpha_2 + \rho_{ce}^3\alpha_3 &= 0 \\ \alpha_1 + 2p_t\alpha_2 + 3p_t^3\alpha_3 &= 0. \end{aligned} \tag{25}$$

The hydrostatic tension apex of the slanted ellipse could be found as the middle root $p_{(2)}$ of the cubic equation $\alpha_0 + \alpha_1 p + \alpha_2 p^2 + \alpha_3 p^3 = 0$ (which must have three real roots as we know). Calculation of this root, however, may be simplified by noting that $p = p_{(3)} = \rho_{ce}$ is also a root. Thus, dividing this cubic equation by $p - \rho_{ce}$, we obtain for the smaller two roots $p_{(1)}$ and $p_{(2)}$ the quadratic equation: $\alpha_3 p^2 + \alpha_4 p + \alpha_5 = 0$, with

$$\alpha_4 = \alpha_2 + \alpha_3\rho_{ce}, \quad \alpha_5 = \alpha_1 + \alpha_2\rho_{ce} + \alpha_3\rho_{ce}^2. \tag{26}$$

By solving this quadratic equation,

$$p_{(2)}, p_{(1)} = -\frac{1}{2\alpha_3}[\alpha_4 \pm (\alpha_4^2 - 4\alpha_3\alpha_5)^{1/2}]. \tag{27}$$

Knowing all the roots, we may check for convexity of the tensile meridian from eqn (7). We should also check that the conditions $\alpha_3 > 0$ and $4\alpha_2^2 - \alpha_1$ are not violated.

To determine the compression meridian, we write the conditions that $p_{(2)}$ and ρ_{ce} as well as the uniaxial compression strength (row 2 of Table 1) must satisfy eqn (11) for the compression meridian, and that the derivative of eqn (11) must vanish for row 6 of Table 1. These conditions furnish the following system of four linear algebraic equations for the unknown constants $\beta_0, \ldots, \beta_3$ of the compression meridian:

$$\begin{aligned} \beta_0 + p_{(2)}\beta_1 + p_{(2)}^2\beta_2 + p_{(2)}^3\beta_3 &= 0 \\ \beta_0 + \rho_{ce}\beta_1 + \rho_{ce}^2\beta_2 + \rho_{ce}^3\beta_3 &= 0 \\ \beta_0 - \tfrac{1}{3}\beta_1 + \tfrac{1}{9}\beta_2 - \tfrac{1}{27}\beta_3 &= \tfrac{2}{9} \\ \beta_1 + 2p_c\beta_2 + 3p_c^2\beta_3 &= 0. \end{aligned} \tag{28}$$

The roots $p_{(1)}$ and $p_{(2)}$ for the compression meridian are the same as for the tensile meridian, but the root $p_{(3)}$ may be different. We can calculate it easily by dividing the cubic equation $\beta_0 + \beta_1 p + \beta_2 p^2 + \beta_3 p^3 = 0$ by $(p - p_{(1)})(p - p_{(2)})$. Then we may check for convexity of the compression meridian from eqn (7).

If the convexity condition, eqn (7), is violated by the tensile or compression meridian, the data in Table 1 must be adjusted. It is quite possible that the data in Table 1 have been estimated with an error, and within the expected scatter range these data may be adjusted. To ensure convexity, one may have to move the dilatancy-free state at tensile or compression meridian (row 5 or 6 of Table 1) upward, i.e. increase r_t or r_c; or increase the value of the biaxial compression strength (row 3); or move the hydrostatic elastic limit to the left (decrease ρ_{ce}); or decrease uniaxial tensile strength (row 1), i.e. decrease ρ_{tc}. In practical experience, however, such adjustments were never needed.

To identify the remaining material constants, one needs to write a computer program which integrates the present constitutive relation. This may be done by using for integration of the present constitutive equation a finite element program with a single finite element. By simulating with this computer program the hydrostatic compression test and the uniaxial compressive and tensile tests, it is possible to obtain parameters λ_1, λ_c and λ_t in a trial-and-error manner. Each of these three parameters may be determined one at a time independently of the others, which is easy to carry out. Parameter Δ_0 may be directly read from the uniaxial compression curve as the horizontal offset of the peak point from the straight line connecting the point $\sigma_1 = 0.6 f_c'$ with the origin. Parameter α may be fixed as $\alpha = 0.2$, although its value may be improved by iterations.

UNLOADING AND RELOADING

The unloading and reloading in the formulation as defined so far is elastic. This will be adequate only for those applications where hysteresis and damage are unimportant. Inelastic unloading can be added to the present model, but how to do it without losing the possibility of sequential identification of material parameters will require further investigation. The most often used approach is a combination of kinematic and isotropic hardening. But for the present model this approach is undesirable because it would make our present sequential identification procedure impossible. A promising choice seems to be the use of contacting nested surfaces of the type introduced by Iwan, Mróz and Prevost because their use would have no effect on the previous response at loading which we have already formulated satisfactorily.

COMPUTER IMPLEMENTATION

The present constitutive model has been implemented at Northwestern University in an explicit dynamic finite element code. Static tests of concrete have been simulated with this code using dynamic relaxation. The calculation proceeds in finite time steps (labeled by superscript n). Due to finiteness of the step, the current stress point is allowed to protrude slightly outside the loading surface. This protrusion is then eliminated in the subsequent iteration by a return to the current loading surface. The method used for the return is the radial return method (see e.g. [33]). The stress state $\hat{\boldsymbol{\sigma}}$ outside the current loading surface must be corrected to the stress $\hat{\boldsymbol{\sigma}} - \Delta\boldsymbol{\sigma}''$. After the correction $\Delta\boldsymbol{\sigma}''$, the loading surface may be approximated according to the Taylor series expansion $\Phi(\hat{\boldsymbol{\sigma}} - \Delta\boldsymbol{\sigma}'') = \hat{\Phi}(\hat{\boldsymbol{\sigma}}) - (\partial\Phi/\partial\hat{\boldsymbol{\sigma}})^T \cdot \Delta\boldsymbol{\sigma}'' = 0$, in which the dot denotes a scalar product of two vectors and $\Phi \equiv F$. It is then assumed that the correction is in the radial direction, i.e. $\Delta\boldsymbol{\sigma}'' = C\hat{\boldsymbol{\sigma}}$, in which C is a constant to be found. Substituting this into the previous condition we can solve the value of C, which yields

$$\Delta\boldsymbol{\sigma}'' = \frac{\Phi(\hat{\boldsymbol{\sigma}})}{\left(\frac{\partial\Phi}{\partial\hat{\boldsymbol{\sigma}}}\right)^T \hat{\boldsymbol{\sigma}}}\hat{\boldsymbol{\sigma}}. \tag{29}$$

These corrections are applied iteratively until the protrusion of the current stress state outside the loading surface meets a given small tolerance.

The computational algorithm in the time step (t^n, t^{n+1}) may be described as follows. Suppose all quantities are known up to time t^n. Given the time step Δt and the incremental nodal displacement Δu, we seek $\boldsymbol{\sigma}^{n+1}$ for each finite element.

1. Evaluate strain increment $\Delta\boldsymbol{\epsilon} = \boldsymbol{B}\Delta\boldsymbol{u}$ and elastic stress increment $\Delta\boldsymbol{\sigma}^e = \boldsymbol{D}^e\Delta\boldsymbol{\epsilon}$. The trial final stress is $\boldsymbol{\sigma}^{n+1} = \boldsymbol{\sigma}^n + \Delta\boldsymbol{\sigma}^e$.
2. $F_1 = F(\boldsymbol{\sigma}^n)$, $F_2 = F(\boldsymbol{\sigma}^{n+1})$. If $F_2 \le 0$, one is still in the elastic range or unloading; go to 5.
3. Find γ such that $F(\boldsymbol{\sigma}^n + \gamma\Delta\boldsymbol{\sigma}^e) = 0$. γ can be determined approximately by a linear interpolation as $\gamma = -F_1/(F_2 - F_1)$. Thus, $(1-\gamma)\Delta\boldsymbol{\sigma}^e$ is the part of loading which should be adjusted according to the loading surface.
4. Evaluate $d\lambda$ from eqn (23). Then compute $\Delta\boldsymbol{\sigma}''$ caused by the strain increment $(1-\gamma)\Delta\boldsymbol{\epsilon}$ and find $\boldsymbol{\sigma}^{n+1} = \boldsymbol{\sigma}^n + \gamma\Delta\boldsymbol{\sigma}^e + \Delta\boldsymbol{\sigma}''$. Then update τ and other parameters. Then adjust the stress value back to the loading surface, i.e. iterate using eqn (29) until $F(\boldsymbol{\sigma}^{n+1}) = 0$.
5. Go to Step 1 and start the next finite element.

COMPARISON WITH TEST DATA

Various typical test data from the literature have been analyzed with the present model in order to assess how closely they can be represented. For this purpose, it has been assumed that the test specimen is in a homogeneous stress state, even though this may be questionable for strain-softening. Thus, the response was calculated using a single finite element, either a unit cubic element with six nodes or an axisymmetric four-node element of square cross-section, each integrated numerically at one point (the center). In simulating the tests that involve strain-softening, the maximum principal strain increments were prescribed for all the loading steps, in order to ensure a stable post-peak response. The material parameter values corresponding to these fits are given in Appendix B.

The uniaxial compression data reported by Hognestad *et al.* [34], van Mier [35] and Kupfer *et al.* [28] are matched in Figs 4(a)–(c), as shown by the solid lines. The data are shown as the data points or the dashed lines. Figure 4(d) shows the fit of the uniaxial tensile test data by Petersson [36].

Figures 5(a) and (b) also show comparisons with biaxial compression data reported by Kupfer *et al.* [28]. Figures 5(c) and (d) show comparisons with the standard triaxial compression tests by Balmer

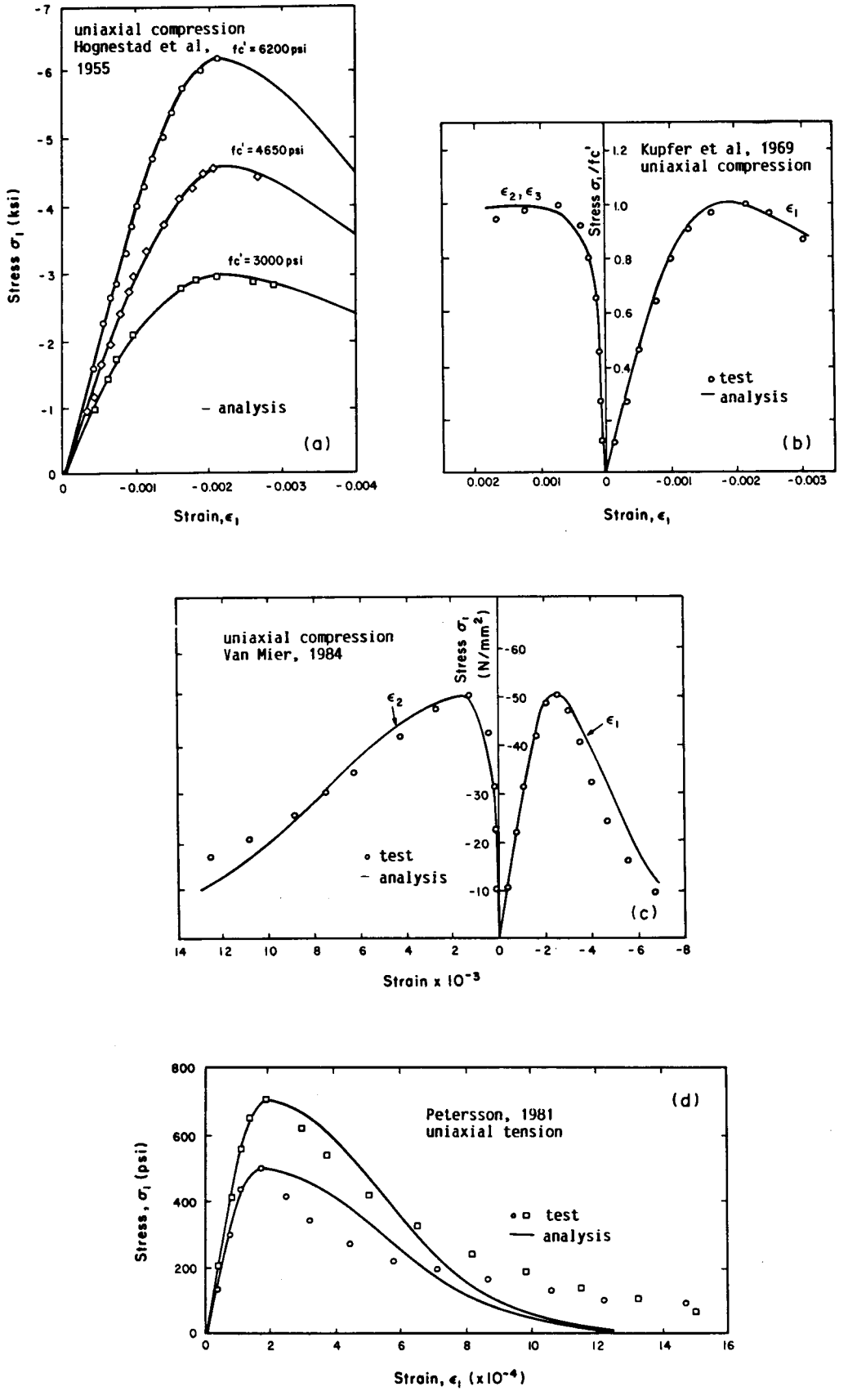

Fig. 4. Fit of uniaxial compression and uniaxial tension data.

[37], and by Kotsovos and Newmann [29]. In these tests, first a hydrostatic pressure is applied, after which one principal stress is increased further. Figure 5(e) shows comparisons with triaxial tests of van Mier [35].

Figures 6(a) and (b) show the fits of the volumetric strain of concrete at uniaxial and biaxial compression. Figure 6(c) shows the comparison with hydrostatic compression data [38]. By fitting these data, the hardening parameter for hydrostatic compression is determined.

Figures 6(d) and (e) show comparisons with test data from cyclic uniaxial and biaxial tests [39, 40]. It is seen that the use of constant elastic moduli in the present theory yields unloading slopes which are much too steep, especially in Fig. 6(d). Improvement could be achieved only by introducing damage-dependent elastic moduli.

The fits of typical test data which can be obtained with the present model are generally quite satisfactory, and are as good as those obtained previously, e.g. with endochronic theory or plastic-fracturing theory, while the identification of the material parameters is here more straightforward.

LOCALIZATION LIMITERS FOR STRAIN-SOFTENING

The present model can be applied in the usual finite element codes only to the extent that no strain-softening takes place. If it does, one must implement some type of localization limiters [41], which prevent localization of strain-softening to a zone of vanishing volume and avoid spurious mesh sensitivity and incorrect convergence. The simplest device to achieve this is to impose a lower limit on the element size, as is done in the crack band model [42]. If the mesh needs to be refined arbitrarily, one can introduce the concept of nonlocal damage in the manner proposed in [43]. This concept means that the parameters of the present model which control strain-softening would have to be expressed from spatial averages of stress and strain taken over a certain representative volume of the material of characteristic size.

CONCLUSIONS

1. The objective has been to find the best possible model which has the following two desirable properties:

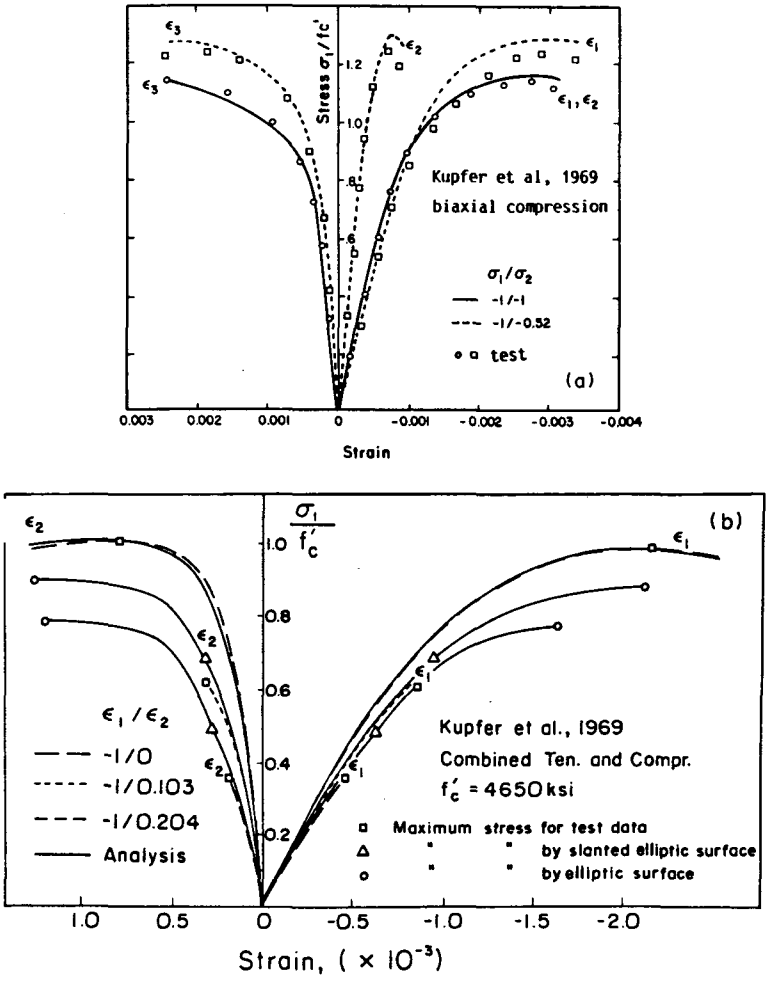

Fig. 5. (a), (b).

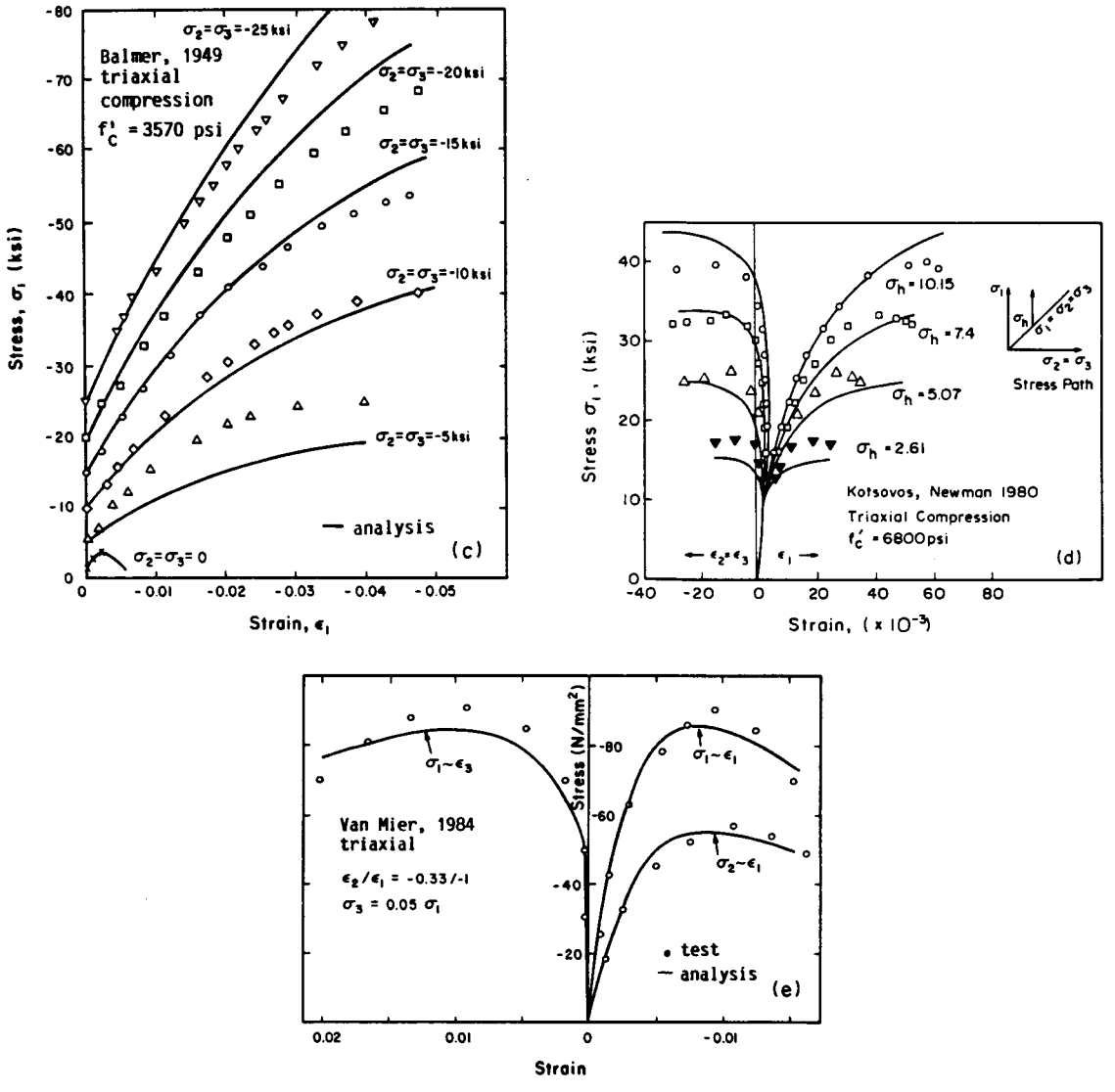

Fig. 5. Fit of biaxial and triaxial data.

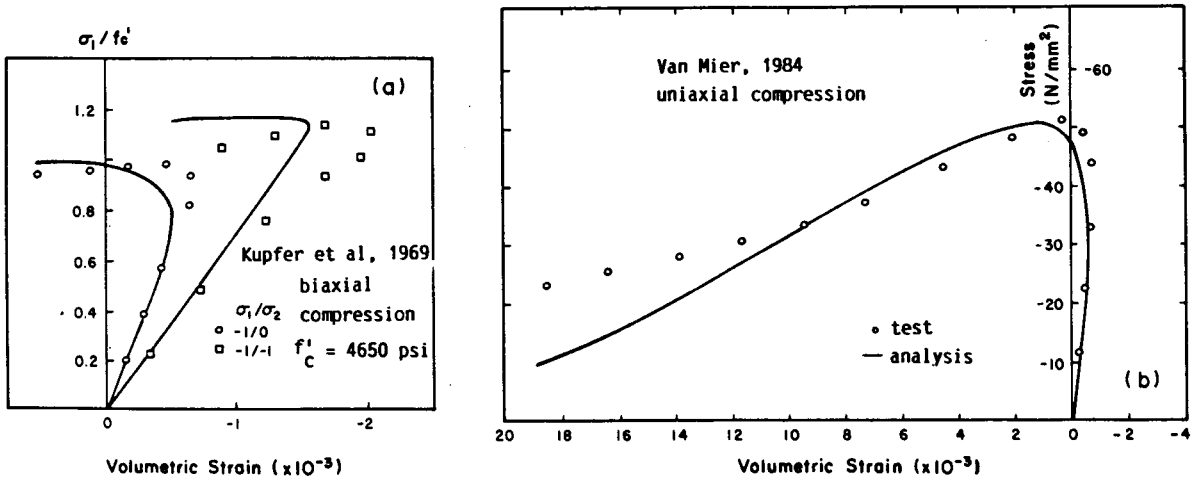

Fig. 6. (a), (b).

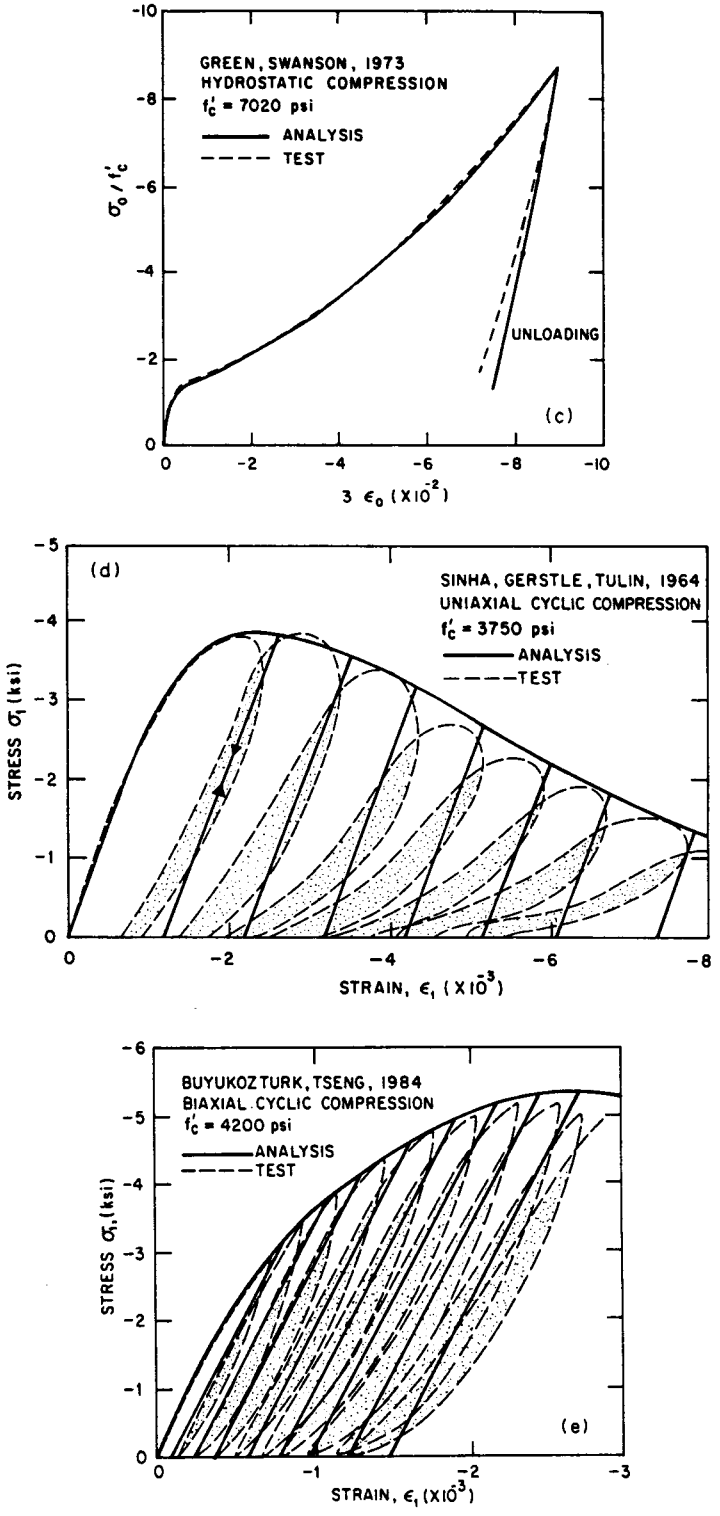

Fig. 6. Fit of volumetric strain, hydrostatic and cyclic data.

(i) It satisfies the classical conditions of plasticity theory desired by numerical analysts: (a) normality (with associativeness), (b) convexity, (c) continuity with regard to subsequent loading surfaces and (d) absence of corners on the loading surface.

(ii) It permits a simple identification of material parameters from the given test data.

2. These conditions are met by developing a loading surface model for which: (a) the deviatoric

cross-sections are rounded triangles; (b) the shear-volumetric (Rendulić) meridians are slanted ellipses; (c) strain-softening is modeled by a reduction of the yield limit; (d) the pre-peak hardening is governed by deviatoric inelastic strain and depends on the similarity angle; (e) the subsequent hardening as well as softening is governed by volumetric inelastic strain. Unloading and reloading are assumed to be elastic in the present form of the model.

3. The principal advantage of the model is that the material parameter identification can be carried out sequentially, rather than by simultaneous nonlinear optimization of the fits of all the data considered collectively. The detailed procedure to do this is given. It involves solution of two systems of four linear equations. The basic experimental information consists of: (a) uniaxial compression strength, (b) uniaxial tensile strength, (c) biaxial compression strength, (d) hydrostatic elastic limit, (e) dilatancy-free states for uniaxial and biaxial compression, (f) strains at uniaxial and biaxial peak stresses.

4. The model agrees well with the basic known test data from monotonic loading tests of concrete.

Acknowledgements—The work was sponsored partly by the U.S. Department of Energy through the Engineering Mechanics Program in the Computational Mechanics Section (J. M. Kennedy, Manager) of the Reactor Analysis and Safety Division at Argonne National Laboratory, and partly by AFOSR Grant No. 83-0009 to Northwestern University.

REFERENCES

1. Z. P. Bažant, A new approach to inelasticity and failure of concrete, sand and rock: enodchronic theory. In *Proc. Soc. Engng Sci. 11th Ann. Mtg* (Edited by G. J. Dvorak), pp. 158–159. Duke University, Durham, N.C. (1974).
2. Z. P. Bažant and P. D. Bhat, Endochronic theory of inelasticity and failure of concrete. *J. Engng Mech. Div. ASCE* **102**, 701–722 (1976).
3. Z. P. Bažant and S. Kim, Plastic-fracturing theory for concrete. *J. Engng Mech. Div. ASCE* **105** 407–428 (1979).
4. Z. P. Bažant and C.-L. Shieh, Hysteretic fracturing endochronic theory for concrete. *J. Engng Mech. Div. ASCE* **106**, 929–950 (1980).
5. Z. P. Bažant and C.-L. Shieh, Endochronic model for nonlinear triaxial behavior of concrete. *Nucl. Engng Design* **47**, 305–325 (1978).
6. Z. P. Bažant and T. Tsubaki, Total strain theory and path-dependence of concrete. *J. Engng Mech. Div. ASCE* **106**, 1151–1173 (1980).
7. O. Buyukozturk and J. Tassoulas, A constitutive model for concrete in compression. *Proc. Third ASCE Engng Mech. Div. Specialty Conf.*, Austin, Texas (1979).
8. C. T. Chen and W. F. Chen, Constitutive relations for concrete. *J. Engng Mech. Div. ASCE* **101**, 465–481 (1975).
9. J. C. Chern and A. H. Marchertas, Private communication (January 1985).
10. H. S. Levine, A two-surface plastic and microcracking model for plain concrete. *Proc. Winter Mtg ASME*, Phoenix, Arizona, pp. 27–47 (1982).
11. F. B. Lin, Private communication on doctoral dissertation in preparation, advised by Z. P. Bažant, Northwestern University (1985).
12. Y. Takahashi, Elastic–plastic constitutive modeling of concrete. ANL 83-23, Argonne National Laboratory (1983).
13. G. Valente, Ultimate strength criteria of concrete under biaxial and triaxial loading. Paper H 2/4, *Proc. 5th Int. Conf. Struct. Mech. in Reactor Technology*, Berlin (1979).
14. B. L. Yang, Y. F. Dafalias and L. R. Herrmann, A bounding surface plasticity model for concrete. *J. Engng Mech. Div. ASCE* **111**, 359–380 (1985).
15. A. Zubelewicz and Z. P. Bažant, Private communication (1984).
16. J. W. Jeter, An evaluation of endochronic concrete theory. Workshop on Constitutive Relations for Concrete, Report of the New Mexico Engng Res. Inst., Albuquerque, N. M. (1982).
17. B. J. Hsieh, On uniqueness and stability of endochronic theory. *J. appl. Mech. ASME* **47**, 748–756 (1980).
18. K. Gerstle *et al.*, Behavior of concrete under multiaxial stress states. *J. Engng Mech. Div. ASCE* **106**, 1383–1403 (1980).
19. J. C. Chern, A. H. Marchertas, Z. P. Bažant and F. B. Lin, Damage-plastic loading surface model for concrete. Report, Argonne National Laboratory, Argonne, Illinois (1986).
20. Z. P. Bažant, Mechanics of distributed cracking. *ASME Appl Mech. Rev.* **39**, 675–705 (1980).
21. Z. P. Bažant, T. B. Belytschko and T. P. Chang, Continuum theory for strain-softening. *J. Engng Mech. Div. ASCE* **110**, 1666–1692 (1984).
22. A. Schofield and P. Wroth, *Critical State Soil Mechanics*. McGraw-Hill, London (1968).
23. P. Launay and H. Gachon, Strain and ultimate strength of concrete under triaxial stress. Paper H1/3, *Proc. Ist Int. Conf. Struct. Mech. in Reactor Technology*, Berlin (1971).
24. G. Gudehus, Elastoplastische Stoffgleichungen für trockenen Sand. *Ing.-Arch.* **42**, 151–169 (1973).
25. J. H. Argyris, G. Faust, J. Szimmat, E. P. Warnke and K. J. Willam, Recent developments in the finite element analysis of prestressed concrete reactor vessels. *Nucl. Engng Design* **28**, 42–75 (1974).
26. F. B. Lin and Z. P. Bažant, Convexity of smooth yield surface of frictional material. *J. Engng Mech. Div. ASCE* **112**, 1259–1262 (1986).
27. K. J. Willam and E. P. Warnke, Constitutive model for the triaxial behaviour of concrete. IABSE Seminar on Concrete Structures Subjected to Triaxial Stresses, Bergamo (1974).
28. H. Kupfer, H. K. Hilsdorf and H. Rüsch, Behavior of Concrete under biaxial stresses. *ACI J.* **66**, 656–666 (1969).
29. M. D. Kotsovos and J. B. Newman, Generalized stress–strain relations for concrete. *J. Engng Mech. Div. ASCE* **104**, 845–856 (1978).
30. E. Melan, Zur Plastizität des raumlichen Kontinuums. *Ing.-Arch.* **9**, 116–126 (1938).
31. Z. P. Bažant, Work inequalities for plastic fracturing material. *Int. J. Solids Struct.* **16**, 873–901 (1980).
32. Z. P. Bažant and B. H. Oh, Microplane model for progressive fracture of concrete and rock. *J. Engng Mech. Div. ASCE* **111**, 559–582 (1985).
33. D. R. J. Owen and E. Hinton, *Finite Elements in Plasticity: Theory and Practice*, pp. 215–219. Pineridge Press, Swansea (1980).
34. E. Hognestad, N. W. Hanson and D. McHenry, Concrete stress distribution in ultimate strength design. *ACI J.* **52**, 455–477 (1955).
35. Jan G. M. van Mier, Strain-softening of concrete under multiaxial loading conditions. Dissertatiedrukkerij Wibro, Helmond (1984).
36. P. E. Petersson, Crack growth and development of fracture zones in plain concrete and similar materials.

Report TVBM 1006, Lund Institute of Technology (1981).
37. G. G. Balmer, Shearing strength of concrete under high triaxial stress-computation of Mohr's envelope as a curve. Structural Research Laboratory Report No. SP-23, Denver, Colorado (1949).
38. S. J. Green and S. R. Swanson, Static constitutive relations for concrete. AFWL-TR-72-2, Air Force Weapons Laboratory, Kirtland Air Force Base (1973).
39. O. Buyukozturk and T. M. Tseng, Concrete in biaxial cyclic compression. *J. Struct. Engng Div. ASCE* **110**, 461–476 (1984).
40. B. P. Sinha, K. H. Gerstle and L. G. Tulin, Stress–strain relations for concrete under cyclic loading. *ACI J.* **62**, 195–210 (1964).
41. Z. P. Bažant and T. B. Belytschko, Strain-softening continuum damage; localization and size effect. Preprints, 2nd Int. Conf. on Constitutive Laws for Engineering Materials, University of Arizona (Edited by C. Desai), pp. 11–33 (1987).
42. Z. P. Bažant and B. H. Oh, Crack band theory for fracture of concrete. *Mater. Struct.* **16**, 155–177 (1983).
43. G. Pijaudier-Cabot and Z. P. Bažant. Nonlocal damage theory. Report No. 86-8/428n, Center for Concrete and Geomaterials, Northwestern University, Evanston, Illinois (1986); *ASCE J. Engng Mech.* **113** (1987) (in press).

APPENDIX A. CALCULATION OF THE DERIVATIVES OF THE LOADING FUNCTION

By chain rule,

$$\frac{\partial f}{\partial \sigma_{ij}} = \frac{\partial f}{\partial \sigma_0}\frac{\partial \sigma_0}{\partial \sigma_{ij}} + \frac{\partial f}{\partial \tau_0}\frac{\partial \tau_0}{\partial \sigma_{ij}} + \frac{\partial f}{\partial \theta}\frac{\partial \theta}{\partial \sigma_{ij}}. \tag{A1}$$

In calculating the derivatives in this expression one needs to note that

$$\partial \sigma_0/\partial \sigma_{ij} = \delta_{ij}/3, \quad \partial \tau_0/\partial \sigma_{ij} = s_{ij}/3\tau_0 \quad \text{and}$$
$$\partial J_3/\partial \sigma_{ij} = s_{ij}s_{kj} - \tfrac{2}{3}J_2\delta_{ij}.$$

APPENDIX B. BASIC INFORMATION ON TEST DATA AND VALUES OF MATERIAL CONSTANTS

1. *Hognestad* et al., *Fig.* 4(*a*), [34].

$\rho_t = 0.1$, $\rho_{cb} = 1.15$, $\rho_{ct} = 1.3$, $\mu = 0.6$, $\lambda_2 = 200$: the coefficients for slanted ellipse are $\alpha_0 = 0.0175$, $\alpha_1 = -0.466$, $\alpha_2 = 0.194$, $\alpha_4 = 0.433$, $\beta_0 = 0.0218$, $\beta_1 = -0.5806$, $\beta_2 = 0.2414$, $\beta_4 = 0.539$.

2. *Kupfer* et al., *Fig.* 4(*b*), [28]

$\rho_t = 0.1$, $\rho_{cb} = 1.15$, $\rho_{ct} = 1.35$, $\mu = 0.6$, $\lambda_2 = 250$, $\alpha_0 = 0.0170$, $\alpha_1 = -0.4501$, $\alpha_2 = 0.1820$, $\alpha_3 = 0.3887$, $\beta_0 = 0.02186$, $\beta_1 = -0.5786$, $\beta_2 = 0.2340$, $\beta_3 = 0.4997$.

3. *Van Mier*, *Fig.* 4(*c*), [35]

$\rho_t = 0.05$, $\rho_{cb} = 1.3$, $\rho_{ct} = 1.7$, $\mu = 0.6$, $\lambda_2 = 200$, $\alpha_0 = 0.00844$, $\alpha_1 = -0.4760$, $\alpha_2 = 0.1709$, $\alpha_3 = 0.2669$, $\beta_0 = 0.01064$, $\beta_1 - 0.6003$, $\beta_2 = 0.2155$, $\beta_3 = 0.3367$.

4. *Petersson*, *Fig.* 4(*d*), [36]

$\mu = 0.60$, $\lambda_1 = 2000$; other coefficients are the same as Hognestad *et al.*

5. *Balmer*, *Fig.* 5(*c*), [37]

$\mu = 0.60$, $\lambda_1 = 200$, $\lambda_2 = 280$; other coefficients are the same as Hognestad *et al.*

6. *Kotsovos and Newman*, *Fig.* 5(*d*), [29]

$\mu = 0.6$, $\lambda_1 = 150$, $\lambda_2 = 280$; other coefficients are the same as Hognestad *et al.*

7. *Green and Swanson*, *Fig.* 6(*c*), [38]

$\mu = 0.6$, $\lambda_1 = 90$; other coefficients are the same as Hognestad *et al.*

8. *Sinha, Gerstle and Tulin*, *Fig.* 6(*d*), [40]

$\mu = 0.65$, $\lambda_2 = 110$; other coefficients are the same as Hognestad *et al.*

9. *Buyukozturk and Tseng*, *Fig.* 6(*e*), [39]

$\mu = 0.65$, $\lambda_1 = 220$.